The CUPID-Mo experiment for neutrinoless double-beta decay search

E. Armengaud[1], C. Augier[2], A. S. Barabash[3], F. Bellini[4,5], G. Benato[6], A. Benoît[7],
M. Beretta[5], L. Bergé[8], N. Besson[1], J. Billard[2], Yu. A. Borovlev[9], Ch. Bourgeois[10],
M. Briere[10], V. V. Brudanin[11], P. Camus[7], L. Cardani[5], N. Casali[5], A. Cazes[2],
M. Chapellier[8], F. Charlieux[2], M. de Combarieu[12], F. A. Danevich[13], I. Dafinei[5],
M. De Jesus[2], L. Dumoulin[8], K. Eitel[14], F. Ferri[1], B. K. Fujikawa[15], J. Gascon[2],
L. Gironi[16,17], A. Giuliani[a,8,18], V. D. Grigorieva[9], M. Gros[1], E. Guerard[10],
H. Z. Huang[19], R. Huang[6], J. Johnston[21], A. Juillard[2], H. Khalife[8], M. Kleifges[26],
V. V. Kobychev[13], Yu. G. Kolomensky[6,20], S.I. Konovalov[3], A. Leder[21], P. Loaiza[10],
L. Ma[19], R. Maisonobe[2], E. P. Makarov[9], P. de Marcillac[8], L. Marini[6], S. Marnieros[8],
X.-F. Navick[1], C. Nones[1], V. Novati[8], E. Olivieri[8], J. L. Ouellet[21], L. Pagnanini[16,17],
P. Pari[12], L. Pattavina[22,23], M. Pavan[16,17], B. Paul[1], H. Peng[19], G. Pessina[16,17], S. Pirro[22],
D. V. Poda[8,13], O. G. Polischuk[13], E. Previtali[16,17], E. Queguiner[2], Th. Redon[8],
S. Rozov[11], C. Rusconi[24], V. Sanglard[2], K. Schäffner[22], Y. Shen[19], B. Schmidt[15],
V. N. Shlegel[9], V. Singh[6], B. Siebenborn[14], S. Sorbino[4,5], C. Tomei[5], V. I. Tretyak[13],
V. I. Yumatov[3], L. Vagneron[2], M. Velázquez[25], M. Vignati[5], M. Weber[26], B. Welliver[15],
L. Winslow[21], M. Xue[27], E. Yakushev[11], V. Yumatov[3], A. S. Zolotarova[8]

[1] IRFU, CEA, Université Paris-Saclay, F-91191 Gif-sur-Yvette, France
[2] Univ Lyon, Université Lyon 1, CNRS/IN2P3, IPN-Lyon, F-69622, Villeurbanne, France
[3] National Research Centre Kurchatov Institute, Institute of Theoretical and Experimental Physics, 117218 Moscow, Russia
[4] Dipartimento di Fisica, Sapienza Università di Roma, P.le Aldo Moro 2, I-00185, Rome, Italy
[5] INFN, Sezione di Roma, P.le Aldo Moro 2, I-00185, Rome, Italy
[6] Department of Physics, University of California, Berkeley, California 94720, US
[7] CNRS-Néel, 38042 Grenoble Cedex 9, France
[8] CSNSM, Univ. Paris-Sud, CNRS/IN2P3, Université Paris-Saclay, 91405 Orsay, France
[9] Nikolaev Institute of Inorganic Chemistry, 630090 Novosibirsk, Russia
[10] LAL, Univ. Paris-Sud, CNRS/IN2P3, Université Paris-Saclay, 91898 Orsay, France
[11] Laboratory of Nuclear Problems, JINR, 141980 Dubna, Moscow region, Russia
[12] IRAMIS, CEA, Université Paris-Saclay, F-91191 Gif-sur-Yvette, France
[13] Institute for Nuclear Research, 03028 Kyiv, Ukraine
[14] Karlsruhe Institute of Technology, Institut für Kernphysik, 76021 Karlsruhe, Germany
[15] Nuclear Science Division, Lawrence Berkeley National Laboratory, Berkeley, California 94720, USA
[16] Dipartimento di Fisica, Università di Milano Bicocca, I-20126 Milano, Italy
[17] INFN, Sezione di Milano Bicocca, I-20126 Milano, Italy
[18] DISAT, Università dell'Insubria, 22100 Como, Italy
[19] Department of Physics, Fudan University, Shanghai 200433, PR China
[20] Physics Division, Lawrence Berkeley National Laboratory, Berkeley, California 94720, US
[21] Massachusetts Institute of Technology, Cambridge, MA 02139, USA
[22] INFN, Laboratori Nazionali del Gran Sasso, I-67100 Assergi (AQ), Italy
[23] Physik Department, Technische Universität Mnchen, Garching D-85748, Germany
[24] Department of Physics and Astronomy, University of South Carolina, SC 29208, Columbia, USA
[25] Université Grenoble Alpes, CNRS, Grenoble INP, SIMAP, 38402 Saint Martin d'Héres, France
[26] Karlsruhe Institute of Technology, Institut für Prozessdatenverarbeitung und Elektronik, 76021 Karlsruhe, Germany
[27] Department of Modern Physics, University of Science and Technology of China, Hefei 230027, PR China

TO DO - PIs: check affiliation of your group.

Abstract CUPID-Mo is a bolometric experiment to search for neutrinoless double-beta decay ($0\nu\beta\beta$) of ^{100}Mo and aims to demonstrate the technology, developed in the framework of the LUMINEU (Luminescent Underground Molybdenum Investigation for NEUtrino mass and nature) project [1], for CUPID (CUORE Upgrade with Particle IDentification) [2–5], a proposed follow-up of the currently running first tonne-scale cryogenic $0\nu\beta\beta$ experiment CUORE (Cryogenic Underground Observatory for Rare Events)[6]. In this article,

[a] e-mail: andrea.giuliani@csnsm.in2p3.fr

we detail the CUPID-Mo detector concept, assembly, installation in the underground laboratory in Modane in 2018, and provide results from the first datasets. The demonstrator consists of an array of 20 scintillating bolometers comprised of enriched 0.2 kg Li_2MoO_4 crystals. The detectors are complemented by 20 thin cryogenic Ge bolometers acting as light detectors to distinguish α from γ/β events by the detection of both heat and scintillation light signals. We observe good detector uniformity, facilitating the operation of a large detector array as well as excellent energy resolution of 5.3 keV (6.5 keV) energy resolution (FWHM) at 2615 keV, in calibration (physics) data. All detectors achieve separation, at 15σ median value, between αs and γ/βs in the region of interest for ^{100}Mo $0\nu\beta\beta$. We present the first limits on the crystals' radiopurity (≤ 3 μBq/kg of ^{226}Ra and ≤ 2 μBq/kg of ^{232}Th). Based on these initial results we also discuss a sensitivity study for the science reach of the CUPID-Mo experiment, in particular, the ability to set the most stringent half-life limit on the ^{100}Mo $0\nu\beta\beta$ decay after a half of year of live-time.

1 Introduction

Two-neutrino double beta decay ($2\nu\beta\beta$) is one of the rarest processes in nature. Initially proposed by Maria Goeppert-Meyer in 1935 [7], it has been observed for 11 nuclei with typical half-lives ranging from 10^{18} to 10^{24} yr [8, 9].

Numerous extensions of the Standard Model predict that double beta decay could occur without neutrino emission (e.g., see [10–14]). This hypothetical transition, called neutrinoless double beta decay ($0\nu\beta\beta$), is a lepton-number violating process. Its signature is a peak in the electron sum-energy spectrum at the Q-value of the transition ($Q_{\beta\beta}$). Its observation could help explain the cosmological baryon number excess [15], and would prove that neutrinos are Majorana fermions (i.e., their own antiparticles) [11, 16].

The current leading $0\nu\beta\beta$ decay experiments have a sensitivity on the $0\nu\beta\beta$ half-life of 10^{25}–10^{26} yr [6, 17–20]. At present, there is no confirmed observational evidence for $0\nu\beta\beta$ decay, which implies that next-generation experiments have to further increase their discovery potential by at least one order of magnitude.

One of the most promising technologies for $0\nu\beta\beta$ decay searches are cryogenic calorimeters, historically also referred to as bolometers [21]. These detectors are sensitive to the minute temperature rise induced by energy deposited in a crystal cooled to cryogenic temperatures (~ 10 mK). Key benefits of bolometers are some of the best energy resolutions in the field (ΔE(FWHM)$/E \sim 0.2\%$), high efficiency, radiopurity, the possibility of particle identification for active background rejection, and versatility in the choice of the material, enabling the study of multiple $0\nu\beta\beta$ decay candidate isotopes [22].

The CUORE experiment [6, 23], currently taking data at Laboratori Nazionali del Gran Sasso (LNGS, Italy), demonstrates the feasibility of a tonne-scale detector based on this technology. The success of this experiment is the starting point of CUPID, which aims to increase the mass of the $0\nu\beta\beta$ decay isotope via isotopic enrichment while decreasing the background in the region of interest.

According to the CUORE background model, the dominant background in the $0\nu\beta\beta$ decay region originates from α particles emitted by radioactive contamination of the crystals or nearby materials [24]. CUPID aims to identify and suppress this background using scintillating crystals coupled to light detectors [25]. A further background suppression can be attained by choosing $0\nu\beta\beta$ decay emitters with a $Q_{\beta\beta}$ well above the 2.6 MeV line of ^{208}Tl, which is typically the end-point of natural γ radioactivity. Bolometers containing isotopes such as ^{100}Mo ($Q_{\beta\beta} = 3034.40(17)$ keV [26]) or ^{82}Se ($Q_{\beta\beta} = 2997.9(0.3)$ keV [27]) satisfy this condition.

The dual readout concept, where both the heat and light signals are recorded, has been implemented in two medium-scale CUPID demonstrators: CUPID-0, taking data at LNGS since 2017, and CUPID-Mo, which started the physics data-taking at the beginning of 2019 in the Laboratiore Souterrain de Modane (LSM, France). Following the CUPID strategy, both experiments make use of enriched crystals (24 $Zn^{82}Se$ crystals for CUPID-0 [28] and 20 $Li_2{}^{100}MoO_4$ crystals for CUPID-Mo) to search for $0\nu\beta\beta$ decay.

With an exposure of ~ 10 kg·yr, CUPID-0 proved that dual readout could suppress the dominant α background to a negligible level, obtaining the lowest background level for a bolometric experiment to date [29]. Nevertheless, the radiopurity and energy resolution (20.05 ± 0.34 keV FWHM at $Q_{\beta\beta}$) of the CUPID-0 crystals [29, 30] do not meet the requirements of CUPID and demand further R&D activity if $Zn^{82}Se$ were to be used.

Conversely, the $Li_2{}^{100}MoO_4$ crystals chosen by CUPID-Mo have demonstrated excellent radiopurity and energy resolution in the tests performed within the LUMINEU collaboration [1, 31]. The primary goal of CUPID-Mo is to demonstrate on a larger scale the reproducibility of detector performance in terms of the high energy resolution and efficient α rejection power combined with high crystal radiopurity. Given the high number of ^{100}Mo emitters contained in enriched crystals, CUPID-Mo also enables a competitive $0\nu\beta\beta$ decay search.

The present work describes the CUPID-Mo experimental setup, currently operating in the EDELWEISS-III [32,

33] cryostat at LSM. The detector was constructed in the clean rooms of the Laboratoire de l'accélélarateur linéaire (LAL) and the Centre de Sciences Nucléaires et de Sciences de la Matiére (CSNSM, Orsay, France) in the Fall of 2017 and then moved to LSM and installed in the cryostat in January 2018. The detector was successfully operated through the Summer of 2018 (Commissioning I). The Fall of 2018 was devoted to cryostat maintenance, after a severe cryogenic failure, and minor detector upgrades. After optimization of the cryogenic system and detectors over the Winter of 2019 (Commissioning II), the experiment has been collecting data in a stable configuration since the end of March 2019 (Physics run). In this paper we present the CUPID-Mo detector concept and construction (Sec. 2), the operation and initial performance of the first Physics run dataset (Sec. 3), and the prospects of the experiment in $0\nu\beta\beta$ decay search (Sec. 4).

2 Experimental setup

CUPID-Mo consists of an array of 20 scintillating bolometer modules arranged in five towers, each with four modules, as shown in Fig. 1. Each module contains one $Li_2{}^{100}MoO_4$ crystal and one germanium wafer assembled inside a single-piece copper housing, instrumented with Neutron Transmutation Doped (NTD) Ge thermistors. All the materials used for the towers' construction were carefully selected, and additionally cleaned as needed to minimize radioactive contamination. The detector construction, transportation, and assembly into the underground cryogenic facility were performed in a clean environment. The key ingredients of the detector, its assembly, and the cryogenic apparatus are detailed below.
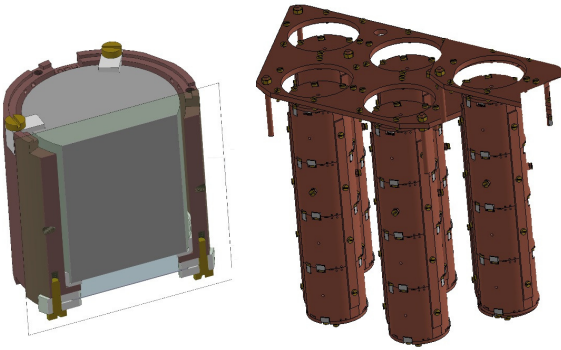

Fig. 1 Rendering of a CUPID-Mo single detector module (left) designed to hold a $Li_2{}^{100}MoO_4$ scintillating element. A module is comprised of a crystal of size ⌀44×45 mm and a Ge wafer of ⌀44×0.175 mm. The full 20-detector bolometric array is arranged in five suspended towers containing four detector modules each (right).

2.1 $Li_2{}^{100}MoO_4$ crystals

CUPID-Mo operates the four existing $Li_2{}^{100}MoO_4$ crystals previously used in LUMINEU [1, 31]. An additional sixteen new $Li_2{}^{100}MoO_4$ crystals were fabricated with the identical procedure as that employed by LUMINEU [1, 34, 35]. All crystals have a cylindrical shape with ~ 44 mm diameter and ~ 45 mm height, and a mass of ~ 0.2 kg. The crystals were produced at the Nikolaev Institute of Inorganic Chemistry (NIIC, Novosibirsk, Russia) as follows:

- purification of the $\sim 97\%$ enriched molybdenum [34], previously used in the NEMO-3 experiment [36];
- selection of lithium carbonate with low U/Th and ^{40}K content [1] and purified ^{100}Mo oxide [35];
- crystal growth via a double crystallization process using the low-thermal-gradient Czochralski technique [1, 35];
- slicing of the scintillation elements, and treatment of their surfaces with radio-pure SiO powder.

The total mass of the 20 $Li_2{}^{100}MoO_4$ crystals used in CUPID-Mo is 4.158 kg, corresponding to 2.264 kg of ^{100}Mo.

2.2 Ge slabs

The high-purity Ge wafers (Umicore Electro-Optical Material, Geel, Belgium), used as absorbers for the scintillation light, have a diameter of 44.5 mm and a 175 µm thickness. A ~ 70 nm SiO coating was evaporated on both sides of the Ge wafer to make them opaque, thus increasing the light collection by $\sim 35\%$ [37]. A small part of the wafer surface was left uncoated to ease the gluing of a temperature sensor.

2.3 Sensors

CUPID-Mo employs NTD Ge thermistors [38] as thermal sensors. These thermistors were provided by the Lawrence Berkeley National Laboratory (LBNL, Berkeley, USA) and come from a single production batch. The NTDs used for the Li_2MoO_4 (LMO) bolometers are $3.0 \times 3.0 \times 1.0$ mm^3 in dimension, and have a temperature-dependent resistance given by $R = R_0 \cdot e^{(T_0/T)^\gamma}$ where the average values for the parameters are $T_0 = 3.8$ K, $R_0 = 1.5$ Ω, and $\gamma = 0.5$. Given the lower heat capacitance of the Ge absorbers, we opted to dice the NTDs used for the bolometric Light Detectors (LDs).

In Commissioning I, we produced three sensors with $3.0 \times 0.8 \times 0.4$ mm^3 dimensions from the slicing of a single NTD in two directions. The LDs with these sensors showed an unexpectedly high noise with a strong $1/f$[Hz] component reaching frequencies up to hundreds of Hz. For Commissioning II and beyond, we replaced all but two sensors

with new ones with $3.0 \times 0.8 \times 1.0 \, mm^3$ dimensions, avoiding the horizontal cut of the original NTDs.

In addition to the thermistor, each $Li_2{}^{100}MoO_4$ crystal is instrumented with a silicon-based resistive chip [39] operated as a heater. This heater allows us to periodically inject a constant power and generate a pulse of constant energy. The resulting reference pulses can be used in the offline analysis to monitor and correct for a change of the signal gain due to temperature drifts of the bolometer [40].

2.4 Sensor coupling

The NTDs were glued on the $Li_2{}^{100}MoO_4$ crystals using the dedicated tool shown in Fig. 2, similar to the one used by CUPID-0 [28]. The glue is a two-component epoxy resin (Araldite® Rapid) suitable for cryogenic applications and demonstrated to have acceptable radiopurity [24]. The gluing tool features a part for holding the NTD, and it can be moved along the vertical axis and fixed at any level. The performance of the bolometer is strongly dependent upon the quality of gluing, and we obtain optimal results when separate glue spots connect the NTD to the crystals. To maintain separate glue spots during and after the epoxy curing, the NTD is kept 50 μm from the Li_2MoO_4 crystal, which is positioned on the top surface of the gluing tool. NTDs of five crystals (LMO-1–4,15), used in the LUMINEU experiment or the CUPID-Mo single tower test, were glued with six spots, while nine spots were applied for the remaining crystals. The heaters were glued with a single glue spot using a 50 μm Mylar mask to provide a gap between the crystal surface and the chip.

The gluing of NTDs to the Ge wafer was also performed with the two-component epoxy resin described above. However, instead of the six or nine spot matrix, we applied a uniform veil of glue. This choice was motivated by the small size of the sensor and the low thermal contraction expected for the Ge-glue-Ge interface. We used the manipulator of an ultrasonic bonding machine to provide a controlled force to attach the NTD to the Ge wafer surface and provide better reproducibility.

2.5 Detector structure

The CUPID-Mo single module and tower structure were designed by the Service de Physique de l'Etat Condensé (SPEC) at CEA, Gif-sur-Yvette, France (Commissariat à l'énergie atomique et aux énergies alternatives) according to the following requirements:

– the single module structure should be compact but permit the housing of four scintillating crystals in a single tower, taking into account the restricted space in the experimental set-up;
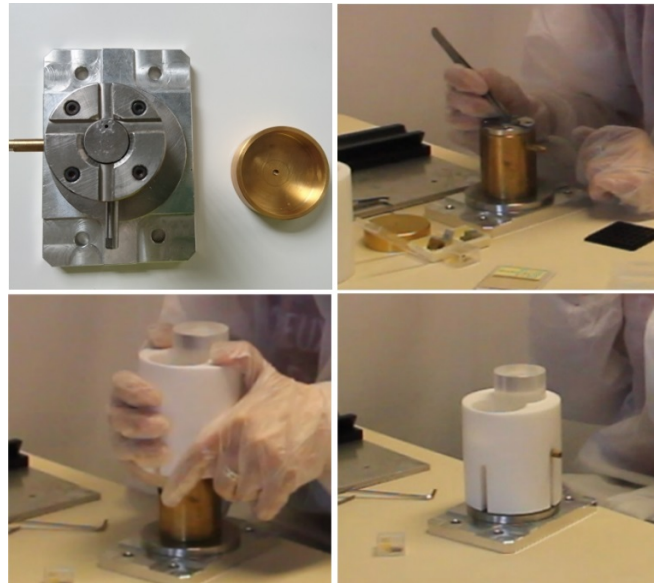

Fig. 2 The tool for gluing the sensor (top left) together with the cap to provide a 50 μm gap. The process of gluing is shown in the three other photos: NTD placement (top right) and placement of the crystal (bottom panels).

– the towers should be suspended by dedicated springs to mitigate the vibrational noise of the set-up [1];
– the design should allow a simple installation inside the cryostat (see Fig. 1 and Sec. 2.8).

The mechanical workshop of LAL (Orsay, France) fabricated the detector support structure. Each detector module (see Fig. 3) is a single-piece holder, made of highly radiopure NOSV^{TM} copper from Aurubis. It contains both a $Li_2{}^{100}MoO_4$ scintillation element and a Ge wafer. The bolometers are kept in place by small Polytetrafluoroethylene (PTFE) holders which decouple them from the thermal bath. The $Li_2{}^{100}MoO_4$ crystals are supported with three PTFE elements on the top and bottom, while the LDs are clamped with three PTFE pieces. In Commissioning I, we did not install any reflector foil around the crystals, because previous measurements demonstrated efficient particle identification performance despite a factor of 2 lower light collection efficiency [22]. Commissioning I was characterized by sub-optimal LD performance (see Sec. 2.3), hence we decided to surround the crystals' lateral side with reflecting foil (3M Vikuiti^{TM}) in addition to the replacement of the LDs' NTDs.

2.6 Detector assembly

We performed all activities related to the detectors' assembly in a cleanroom environment. All the used detector components were carefully cleaned before assembly to minimize the risk of surface re-contamination. In particular, cop-
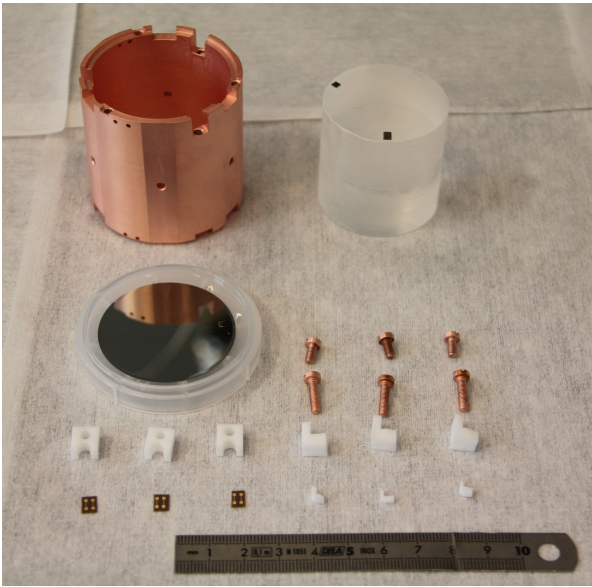
Fig. 3 All components used to assemble a CUPID-Mo single detector module: a copper holder, a $Li_2{}^{100}MoO_4$ crystal with glued NTD and heater, a Ge LD with NTD, the copper screws, the PTFE spacers and fixing elements, the Kapton foil with golden pads. Note that the reflecting film is not shown here.
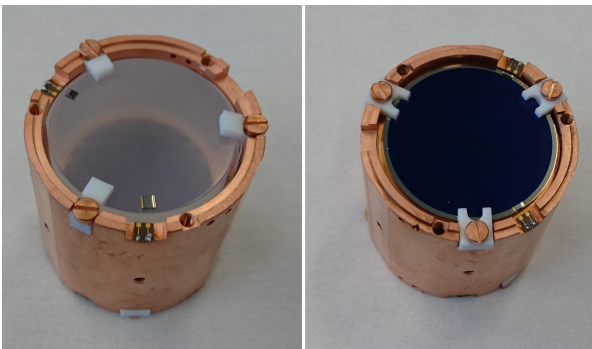

Fig. 4 An assembled CUPID-Mo module. On the left: view from the top, the semi-transparent crystal surface where the NTD and heater are located. On the right: view from the bottom, germanium LD with SiO coating (dark blue internal circle); the 2 mm on the edge of the wafer (17% of the area) are uncoated.

Fig. 5 Twenty CUPID-Mo detector modules before their arrangement in five towers; the devices are shown from the $Li_2{}^{100}MoO_4$ crystal side (top) and from the Ge LD side (bottom).

Fig. 6 The five assembled towers before installation in the cryogenic facility.

per elements were etched with citric acid, and PTFE elements cleaned with ethanol in an ultrasonic bath. The tower assembly was performed in a class 10 cleanroom at LAL. The Li_2MoO_4 crystal is fixed inside its copper housing with PTFE elements on top and bottom as well as surrounded by a reflecting foil. An assembled single module (top and bottom view), as well as all the CUPID-Mo detectors, are shown in Fig. 4 and Fig. 5, respectively. In total, five towers were assembled with four detectors each (Fig. 6). Crystals on the lower three floors are each viewed by one LD from the top and one LD from the bottom. The top floor crystals are each viewed by one LD from the bottom.
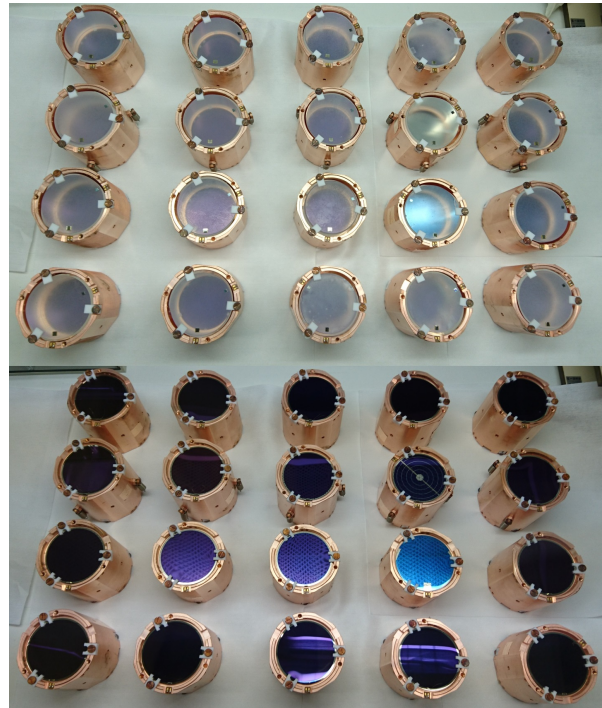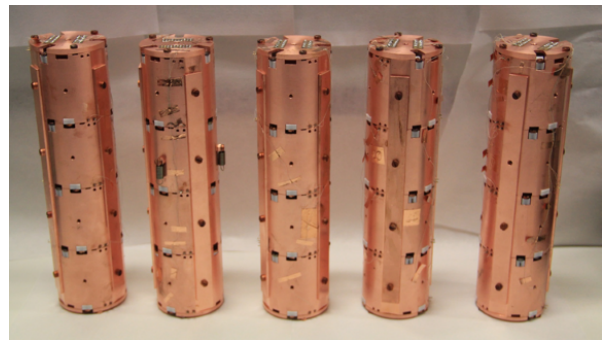
2.7 Wiring

A dedicated wiring scheme was designed and implemented for the CUPID-Mo experiment as the existing EDELWEISS-III readout could not accommodate the additional 20 dual-readout modules required for CUPID-Mo.

We bonded gold wires from the NTDs to flat Kapton cables with gold contacts to provide the electrical readout connection as well as the weak thermal link to the heat bath. Silk-covered constantan twisted wires were soldered on the other side and run up each tower to a larger Kapton pad with gold contacts glued at the top of the tower.

On this pad the constantan wires and copper wires (connection to the cold electronics) were soldered[1]. This connection provides a link to Si-JFET (junction gate field-effect transistor) based pre-amplifiers at 100 K through the copper plate inside the EDELWEISS cryostat (see Sec. 2.8).

2.8 Low background cryogenic facility

The CUPID-Mo detector array is installed (see Fig. 7) in the EDELWEISS-III cryogenic set-up [1, 32], located in LSM. This site is among the deepest underground laboratories in the world; the 1700 m (4800 m water equivalent) rock over-burden, provided by the Frejus mountain, reduces the cosmic muon flux to 5 muons/m^2/day [41].

The EDELWEISS cryostat is a custom dilution refrigerator with a reversed geometry [32], developed by Institut Néel (Grenoble, France). During a cryogenic run, this set-up requires periodic refilling of the liquid helium (LHe) bath every 10 days. The consumption of LHe is minimized by the use of a cold vapor reliquefaction system based on three Gifford-MacMahon cryocoolers. The cryocoolers are responsible for most of the vibrational noise in the set-up, thus necessitating the use of the suspension to achieve high-performance operation of the scintillating bolometers [1]. The passive shielding of the set-up against environmental radiation consists of lead (20 cm thickness) and polyethylene

(55 cm thickness). The inner part of the lead shield is made of 2 cm thick low ^{210}Pb radioactivity (< 0.12 Bq/kg) lead recovered from sunken Roman-era galleys (here on to called "Roman lead"). An additional internal Roman lead (14 cm) and polyethylene (10 cm) shield at the 1K-plate is used to protect the detectors from radioactivity from the cryostat components. A muon veto system is surrounding the whole cryostat providing 98% geometrical coverage. The muon veto is constructed from 46 individual plastic scintillator modules with a total surface of 100 m^2 and provides a detection efficiency of 97.7% for central muons [41]. The set-up is located inside a class 10000 cleanroom with a depleted radon air supply ($\sim$30 mBq/m^3 of ^{222}Rn).

---

[1]Later, high purity Ge counting (HPGe) revealed that the solder is not Pb-free (the activity of ^{210}Pb is (170$\pm$15) Bq/kg); the total mass of the material on the towers is (1.2$\pm$0.1) g.

Table 1 CUPID-Mo tower compositions and their corresponding slots inside the EDELWEISS set-up at LSM.

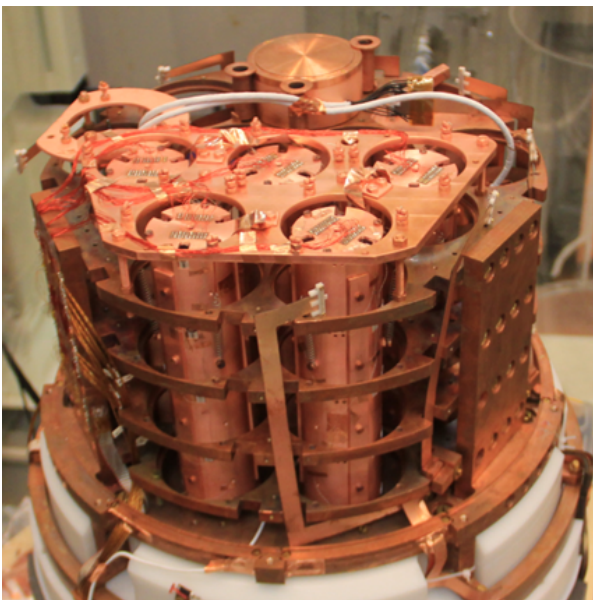| Tower composition	Detectors' IDs and towers' slots				
	T3	T4	T10	T11	T12
LMO LD	5	9	17	2	13
LMO LD	6	10	16	3	18
LMO LD	7	11	14	4	19
LMO LD	8	12	1	15	20

Fig. 7 The CUPID-Mo scintillating bolometer array installed inside the EDELWEISS set-up. The remainder of the experimental volume is occupied by eleven Ge-based bolometers of the EDELWEISS direct dark matter search experiment and one scintillating bolometer for CUPID R&D.
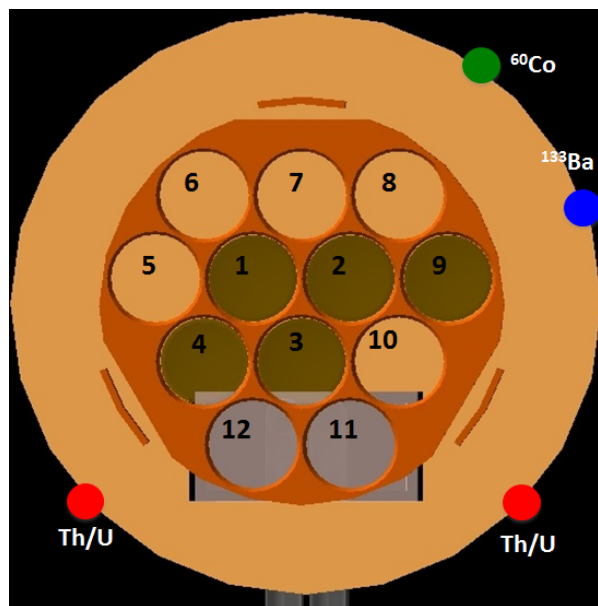

Fig. 8 A schematic top view on detectors plate inside the EDELWEISS set-up showing twelve slots for tower installation inside copper plates. The position and types of calibration sources are also indicated.

The experimental volume of EDELWEISS-III contains four floors (detector plates) with twelve slots each (see Fig. 8). The CUPID-Mo towers were inserted through the slots T3, T4, T10, T11, and T12 (see Table 1) and mechanically decoupled from the EDELWEISS-III detector plate with three metal springs for each tower[2]. The remaining experimental space is partially occupied (tower slots T2, T5, T7, and T8) by 11 Ge bolometers for the EDELWEISS dark matter search program [42] and a cadmium tungstate based scintillating bolometer for CUPID R&D [43].

We added two mixed U/Th sources made of thorite mineral to the EDELWEISS-III automatic source deployment system [32] (see Fig. 8). These sources complement the already available γ-calibration sources of ^{133}Ba ($\sim$1 kBq) and ^{60}Co ($\sim$100 kBq) for periodic calibration of the CUPID-Mo detectors. The activities of the sources are $\sim$50 Bq of ^{232}Th, $\sim$100 Bq of ^{238}U, and few Bq of ^{235}U. The ^{133}Ba source emits γs with energies up to 400 keV and was only used during the commissioning stage. The high-activity ^{60}Co γ source is used to eliminate space charges in the dual readout heat-ionisation Ge bolometers of EDELWEISS-III [32] and also to calibrate the CUPID-Mo Ge LDs via source-induced X-ray fluorescence [44, 45] (see Sec. 3.3). The ^{60}Co source is used mainly during and just after each LHe refill (every 10 days) while a regular $\sim$2-days-long Th/U calibration is scheduled for each period between subsequent LHe refills.

The detector readout in the EDELWEISS-III setup is based on AC-biased cold electronics [32], which restricts the use of high-resistivity thermistors to at most a few MΩ resistance at a given bias current (working point) [1]. Custom made room-temperature electronics modules called bolometer boxes (BBs) are mounted just outside of the cryostat to ensure short cables to limit noise pick-up. These BBs contain the electronics for the cold Si-JFET pre-amplifiers' biasing, Digital to Analog Converters (DACs) for the detectors' biasing, post-amplification, anti-aliasing filter, and ADCs to record the CUPID-Mo NTDs [32]. All LMOs and five LDs are operated with BBs containing 16-bit ADCs, while the signal digitization for the remaining LDs is done with 14-bit ADCs. The pulser system, used to inject a constant Joule power through the heaters, is based on a 4-channel pulse generator with a typical injection periodicity of a few minutes. The data acquisition system [1, 32] can record both online triggered and stream data; the triggered data is used only for monitoring purposes.

3 CUPID-Mo operation and performance

3.1 CUPID-Mo detector operation

Of the 20 LMO and LD pairs, only a single LD was lost due to a hardware issue, resulting in 39 out of 40 active channels. Additionally, 18 out of 20 heaters are available to inject pulses. The optimal working point of the LMO detecotrs was chosen to maximize the signal amplitude. LDs, instrumented with smaller, more resistive, sensors operate in an over-biased regime to obtain an NTD resistance of $\sim$1 MΩ mitigating the impact of AC biasing (see details in [1]). The modulation frequency of 500 Hz was chosen to reduce the pick-up of cryocooler-induced high-frequency noise[3]. The nominal base temperature of the empty EDELWEISS cryostat is 11.5 mK. In the present, densely populated, cryogenic setup, an additional heat load increases this base temperature to $\sim$20 mK and we could stably operate at 20.7 mK with a few μW of regulation power. This temperature is considerably higher than the operating temperature in the LUMINEU predecessor [1] and it is expected to have an adverse effect on the detector performance.

Nevertheless the following analysis of a $\sim$ 2 week period with 11.1 days of physics data, 2.2 days of mixed Th/U source calibration, and 1.6 days of ^{60}Co irradiation provides a robust confirmation of the bolometric performance achieved within LUMINEU [1, 22]. The data were acquired between March 24th and April 6th and correspond to a physics exposure of 0.1 kg×yr. This early data is comparable with the prior exposure presented in [22], and emphasizes the reproducibility of Li$_2$MoO$_4$ detectors using a total of 20 detectors.

3.2 Data processing

Two independent analysis frameworks, both exploiting the optimum filter technique [46], are used for the data processing: one, called Diana [47, 48], is adapted from the CUORE [6] and CUPID-0 [48] experiments and the other was developed at CSNSM [49] and used for the analysis of the LUMINEU data [1]. The CSNSM code has been developed (using the MATLAB MULTI Integrated Development Environment) specifically for the analysis of scintillating bolometer data. It is more nimble and readily adapted to different experimental setups. In contrast, Diana is a much broader framework, including analysis packages for larger detector arrays (in particular allowing for the analysis of coincident events). It is object-oriented C++ code with a PostgreSQL [50] database interface to track detector and electronics settings. The use of Diana allows for comparison between dif-

---

[2]The activity of ^{228}Th and ^{226}Ra and ^{60}Co in the springs is $\sim$0.01 Bq/kg, while the ^{40}K content is $\sim$4 Bq/kg; the total mass of the material is around 8 g.

[3]A better noise environment was observed using the EDELWEISS wiring [32] in LUMINEU allowing for a 1 kHz modulation frequency [1, 31].

ferent CUPID project demonstrator experiments with effectively the same analysis tools, and Diana is expected to be used as the primary package for CUPID-Mo in the future. Therefore, all results presented below are based on the use of Diana, while it is noted that very similar results were obtained with the CSNSM code, providing a cross-check of the Diana processing.

3.3 Performance of bolometric Ge light detectors

Characteristic pulse shape parameters such as the rise- and decay-times, defined as 10% to 90% of the rising edge and 90% to 30% of the trailing edge of the LD pulse shape have been investigated (see Table 2). We estimate typical (median) rise- and decay-times of 4.2 ms and 9.2 ms respectively from an averaged pulse, triggered and aligned on events recorded in an associated LMO crystal.

Averaging of pulses was necessary since Li_2MoO_4 has a moderate Relative Light Yield (RLY) which does not exceed 1 keV/MeV relative to the heat signal (see [1, 31] and Sec. 3.4), and estimates from individual light pulses are subject to bias from noise fluctuations. We note that in particular for the rise-time both the 500 Hz sampling and the alignment of the average pulse become limiting factors for a more precise estimate. At a previous surface test at CSNSM with a similar temperature, working point, and a 10 kHz sampling rate, a factor of 3 faster rise-time (0.96 ms) was observed in LD4.

To estimate the performance of the Ge LDs, we perform an in situ calibration. We employ the X-ray fluorescence of Mo or Cu that is generated when the crystals and setup are exposed to a higher intensity γ source [44, 45]. For Mo we expect characteristic peaks from the $K_{\alpha 1}$ (17.48 keV, intensity $I = 100\%$), $K_{\alpha 2}$ (17.37 keV, $I = 52\%$), and $K_{\beta 1}$ (19.61 keV, $I = 15\%$) lines [51]. The Cu X-rays can give additional peaks from $K_{\alpha 1}$ (8.05 keV, $I = 100\%$), $K_{\alpha 2}$ (8.03 keV, $I = 51\%$), and $K_{\beta 1}$ (8.91 keV, $I = 17\%$). Fig. 9 shows a typical X-ray spectrum obtained during the ^{60}Co source irradiation. The prominent features are a sum K_α peak from Cu and both a sum K_α and a distinct K_β peak from Mo. The intensity of the Cu X-rays is much lower than those associated with Mo, as the Cu is only facing the LDs on the side. Also, the statistics in the Cu K_α peak are very low for detectors far from the ^{60}Co source, and we choose to omit this peak from the LD calibration.

With a stable operating temperature of 20.7 mK and a strong NTD polarization for the Ge LDs, negligible nonlinearity is expected. We use a Gaussian fit to the most intense peak, the Mo K_α X-rays, and perform a first-order polynomial calibration with zero intercepts.

The 1.4 g Ge LDs are instrumented with small-size NTDs that achieve a typical sensitivity of 1.1 μV/keV with an RMS of $\sim 40\%$ (see Table 2). Uncertainties in the individual sensitivity estimates are dominated by the gain in the analog

Table 2 Performance of Ge light detectors of the CUPID-Mo experiment. Detectors marked with an asterisk (*) suffer from additional uncertainty due to prominent sinusoidal noise. The quoted parameters are the NTD resistance at the working point (R_{work}), the rise time (τ_R), the decay time (τ_D), the voltage sensitivity (A_{Signal}), and the baseline noise resolution (FWHM$_{Noise}$). For the definition of the listed variables see text.

| LD ID	R_{work} (MΩ)	τ_R (ms)	τ_D (ms)	A_{Signal} (μV/keV)	FWHM$_{Noise}$ (eV)
1	1.18	5.0	8.3	0.5	183
2	0.87	3.6	9.2	1.2	92
3	0.37	3.3	5.6	0.5	1225
4	0.92	3.2	8.5	1.7	175
5	0.75	3.5	9.9	1.1	66
6	0.70	3.8	9.5	1.0	175
7	–	–	–	–	–
8	0.50	3.8	3.6*	0.7	368
9	0.95	3.6	4.7*	1.0	354
10	0.91	3.5	5.2*	1.1	323
11	1.83	4.5	4.2	2.6	146
12	0.86	5.2	18.0	1.0	69
13	0.70	9.7	11.5	1.3	112
14	0.90	9.0	10.2	1.2	122
15	0.77	4.3	14.1	1.2	86
16	0.46	4.2	9.4	0.8	219
17	0.73	4.2	7.2	1.3	129
18	0.66	4.1	9.3	1.2	121
19	0.76	4.3	9.0	1.2	202
20	1.14	4.9	23.5	0.6	137
Median	0.77	4.2	9.2	1.1	146
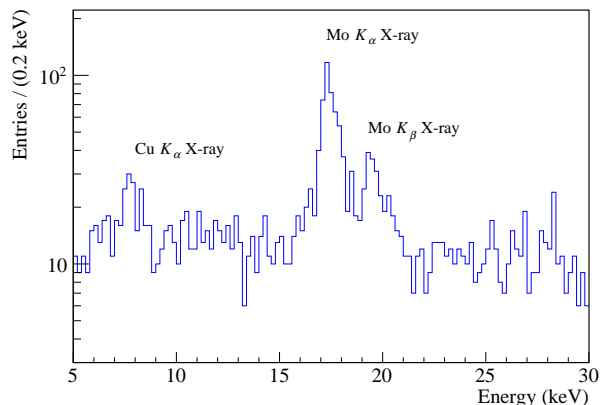
Fig. 9 Energy spectrum of CUPID-Mo light detector LD2 after a 33 h ^{60}Co irradiation in the EDELWEISS-III set-up. The Mo K_α X-rays are used for the LD calibration.

chain with typical uncertainties of order 10% for several of the operational amplifiers in the amplification chain. The LDs sensitivity is limited by a comparatively high regulation temperature of the detector plate and the strong NTD polarization[4].

---

[4] A factor of two higher signal amplitude in LD4, operated at 17 mK, was observed in an surface test at CSNSM (see Fig. 23 in [5]).

We estimate the baseline resolution for all detectors from a set of forced random trigger events injected every 101 s. We exclude one detector instrumented with a different NTD sensor (used in Commissioning-I), see Table 2 and runs with atypical noise performance, resulting in 183/209 (LD-bolometer, run) pairs. The median of these estimates yields a typical baseline resolution of 148 eV FWHM in agreement with the channel based estimate in table 2. We see good reproducibility with individual channel estimates ranging from 66 eV up to 368 eV.

A resulting scatter plot of the correlation between the sensitivity and the achieved baseline resolution is shown in Fig. 10. We note that the spread in detector performance is only slightly higher than for the NTDs on the Li_2MoO_4 crystals (see Sec. 3.4). We want to emphasize the uniformity that lends itself to applications in larger cryogenic detector arrays.
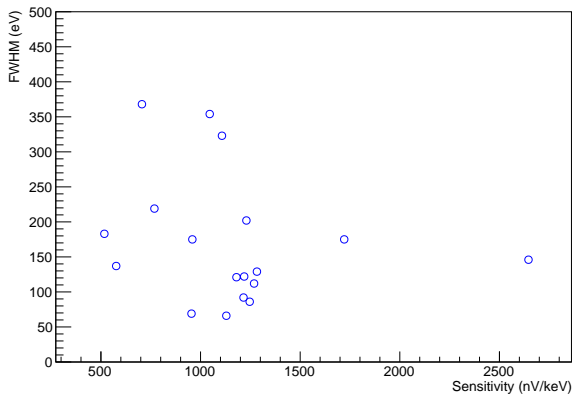
Fig. 10 The baseline resolution versus sensitivity for 18/20 Ge LDs operated in the CUPID-Mo experiment at 20.7 mK. One detector is discarded due to having a different NTD, while the second is not operational (see text).

For reference, we list the performance characteristics on an individual LD basis in Table 2. The reported performance in terms of the baseline resolution exceeds the requirements to achieve a better than 99.9% rejection of α events at 99.9% acceptance of γ/βs as is discussed in detail in Sec. 3. Several improvements can be pursued for the full-size CUPID experiment. DC-biased electronics, higher sampling rate, and the implementation of additional analysis and de-noising techniques can improve the quoted performance. Futhermore, lower noise NTD Ge sensors and a lower operational temperature resulting in a higher detector sensitivity can also yield a significantly better LD performance, as demonstrated with a 20 eV FHWM Baseline resolution in [52].

3.4 Performance of $Li_2{}^{100}MoO_4$ bolometers

The time constants of LMO bolometers are much longer than those of LDs. We obtain median values of 24 ms for the rise-time and 299 ms for the decay-time with a significant spread of 208 ms in the decay-times and a smaller spread of 8 ms in the rise-time (see Table 3). These values are consistent with previously reported values [1], and in the typical range for macroscopic cryogenic bolometers operated in the tens of mK range.

We calibrate with a mixed Th/U source, with a most prominent peak at 2615 keV (^{208}Tl) and negligible gamma continuum, see Fig. 13. This is the closest observable γ-line, ~ 415 keV lower than the $Q_{\beta\beta}$-value of ^{100}Mo.

The calibration data were acquired over a short period (2.2 days), resulting in limited statistics of the detected γ peaks. We neglect nonlinearities in the detector response and fit using zero and the 2615 keV ^{208}Tl line. Additionally, we use this peak to correct for changes in thermal gain due to slow temperature drifts in the experimental setup. The resulting correction is a linear scaling factor obtained from the optimum filter (OF) amplitude versus baseline dependence in the calibration data and is applied to both calibration and background data.

The detector sensitivity at the 20.7 mK operation temperature has a median value of 17 nV/keV with an RMS of about 30% (see Table 3). For unknown reasons, the detector LMO 2 shows very low sensitivity in comparison to the results of the CUPID-Mo Commissioning-I (6 nV/keV at 20.5 mK) and LUMINEU (47 nV/keV at 17 mK [44]). As in the case of LDs, larger sensitivity of LMO bolometers is expected at colder temperatures (e.g., compare results given in [1]).
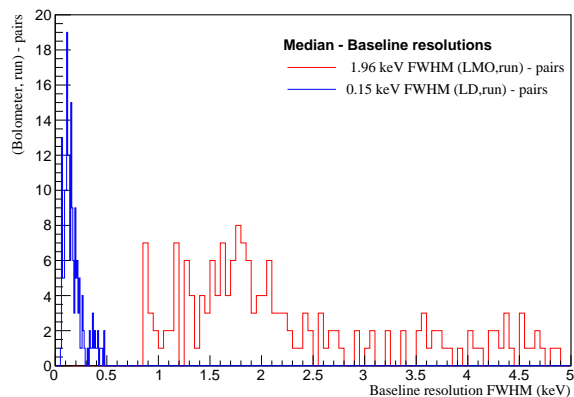

Fig. 11 Baseline resolution (FWHM) distributions for 183 (LD, run) and 189 (LMO, run) pairs. LMO 2 and LD 3 are rejected, as are periods with atypical noise.
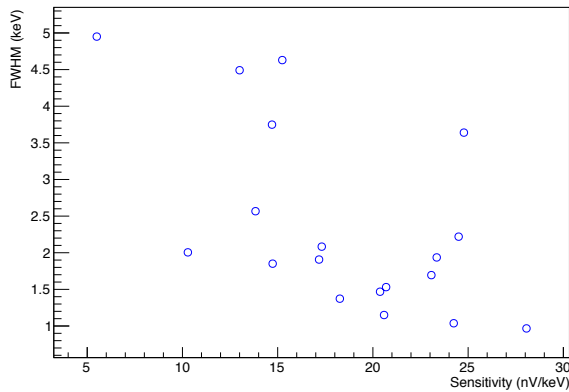
Fig. 12 Sensitivity versus baseline resolution (FWHM) for the 19 LMO detectors considered in this analysis. One detector (LMO 2) is omitted due to abnormal performance; see text).
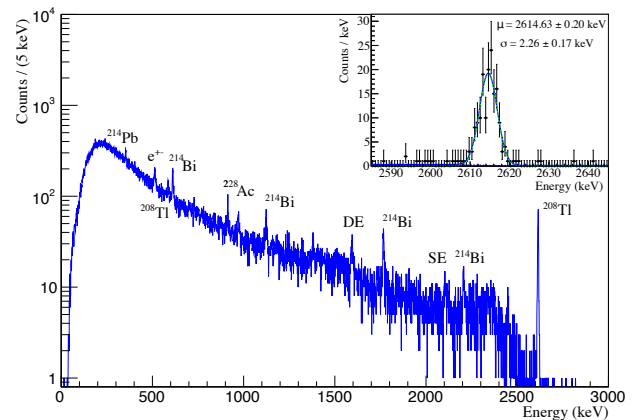

Fig. 13 Summed calibration spectrum for 19/20 Li_2MoO_4 bolometers. All the major peaks have been labeled. The inset shows a fit of the ^{208}Tl γ peak at 2614.5 keV.

The same method utilized for the investigation of LDs' baseline resolution (see Sec.3.3) is also applied for Li_2MoO_4 bolometers. We obtained characteristic (median) values of 1.96 keV FWHM for the baseline resolution with the spread of the distribution given in Fig. 11 and individual detector based resolutions presented in Table 3. The baseline noise versus sensitivity data is also illustrated in Fig. 12.

For further analysis, we utilize a preliminary set of analysis cuts. First, periods of atypical noise and temperature spikes of the cryostat are rejected, removing $\sim$11% of the data from the commissioning period. A large part of the loss of livetime is caused by a suboptimal setting of the cryostat suspension, and improved stability has been observed in more recent data[5]. We exclude pile-up events with another trigger in a $(-1, +2)$ s window, require a baseline slope consistent with the typical behavior of the channel, and require both the rise-time as well as the optimum filter peak position to be within 5 median-absolute deviations (MAD) of the mean range as defined by the overall distribution of these values. We further select γ/β events by requiring events to have a RLY (see Sec. 3.5) within 4σ of the mean amplitude incident in a LD associated with a LMO bolometer.

The resulting calibration data is presented as a summed spectrum in Fig. 13. The 2615 keV ^{208}Tl resolution is 5.3 keV (FWHM) estimated with an unbinned extended maximum likelihood (UELM) fit shown in the inset. The fit model includes a Gaussian function and two components, a smeared step function for multi-Compton events and a locally flat background. We note a potential bias on the resolution since we perform the thermal gain stabilization on this gamma peak and are in a low statistics limit. A toy Monte-Carlo (MC) with a typical value of 20 counts per detector resulted

in an estimated bias (underestimate of the ^{208}Tl peak width) of 0.3 keV.

In addition to the good energy resolution, we highlight the linearity and uniformity of the data. The maximum residual between observed peak position and expected peak position in the summed calibration spectrum was 3 keV for the 1120 keV line from ^{214}Bi. Similarly, we observe an excess width for all γ peaks of at most 5 keV due to not yet accounted for individual detector non-linearities.

3.5 Performance of light-vs-heat dual readout

We estimate the RLY from events in the 2–3 MeV region, close to the Q-value for $0\nu\beta\beta$ of ^{100}Mo. We create a distribution light/heat energies and fit a Gaussian to this distribution to obtain the RLY μ_γ for γ/β events. We obtain 31 individual (LMO, LD) pairs comprised of 15 LMOs in the line of sight of two LDs (minus a failed, and an underperforming LD) and 5 LMOs with a direct line of sight to a single LD (see Sec. 2.6).

The resulting RLYs (in keV/MeV) are listed in Table 3 and illustrated in Fig.14. The predicted RLY includes both the effect of scintillation light production in the crystal as well as light propagation to the Ge absorber, and a pattern that is dominated by the latter effect emerges. $Li_2^{100}MoO_4$ crystals on the top of the towers with a reflective copper cap at the upper side and a single LD at the bottom, observe the highest LYs with a median value of 0.90 keV/MeV. In addition a $\sim$0.1 keV/MeV difference is observed in light collection between the top (0.74 keV/MeV) and the bottom (0.64 keV/MeV) LDs. This effect is a result of a protrusion that is part of the crystal support, which acts as an aperture for downward going light. The obtained results are consistent with previous observations [1, 31]. The summed light
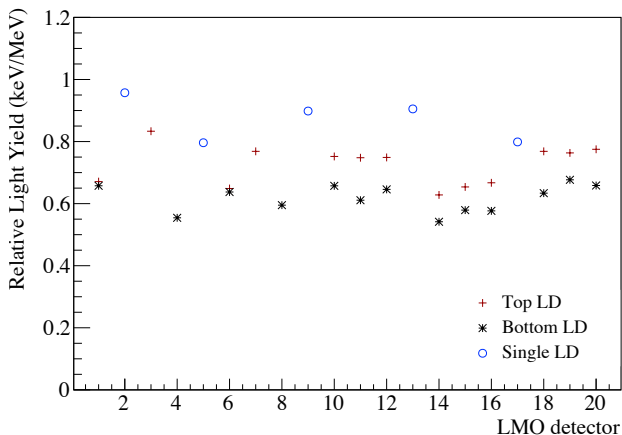
---

[5]$\sim$ 95% of the data are kept after the data quality selection since April 2019

Fig. 14 Relative Light Yields for all of the Li$_2$^{100}MoO$_4$ crystals. The differences in RLY trace the expected light collection efficiencies due to the design of the towers, see Sec. 2.5 and 2.6.

collected from two adjacent LDs is the closest estimate we have for ideal light collection. It is as high as 1.44 keV/MeV with a median value of 1.35 keV/MeV. The uncertainty for individual RLY estimates has been quantified from the spread in RLY estimates of three distinct ^{60}Co plus ^{208}Tl datasets. We observed a ∼4% spread around the mean (RMS), with a maximum deviation of 16% for a single detector.

For this analysis, we opt to use the LD in the same detector module just below the crystal by default. In cases where the lower LD is unavailable or performs significantly worse (LMO 1,3,6 and 7) we switched to associating the upper LD to this crystal (see also Tables 2 and 3).
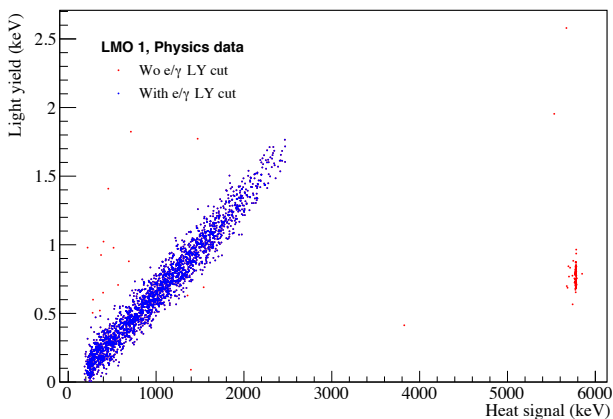
Fig. 15 Light yield versus heat signal scatter-plot using 11 days of physics data from LMO 1. The presented detector has the highest ^{210}Po contamination to illustrate best the distributions of α and γ events and the scintillation light quenching for α events.

Taking into account the measured RLY (Table 3) and the LD performance (Table 2), all detectors achieve better than

99.9% discrimination of α events (see sec. 3.6) with a typical example of the discrimination power given in Fig. 15. The preliminary γ/β selection by RLY (blue) defined before eliminates all α events (red), which exhibit about 20% of the RLY of γ/β events. This particular crystal is characterized by the highest contamination level of ^{210}Po with ∼ 0.5 mBq/kg and hence best exemplifies the alpha discrimination power achieved for a scintillating bolometer with typical performance values of 0.67 keV/MeV RLY and 0.18 keV FWHM$_{Noise}$ of a coupled LD. We observe that the ^{210}Po α events misreconstructed at ∼7% higher energy at 5.8 MeV instead of 5.4 MeV. This shift is much larger than nonlinearities in the γ region would suggest, but we note that a similar difference in the detector response for alpha particles has been observed previously with lithium molybdate based detectors [1, 31].

We estimate a scintillation light quenching of α-particles with respect to γ/β particles of $(19.8 \pm 1.1)\%$ across the detectors (see Table 3). These results are also within expectations for this scintillation material [1, 22, 31].

3.6 Extrapolated α discrimination of Li$_2$^{100}MoO$_4$ scintillating bolometers

We systematically evaluate the α discrimination level following Refs. [1, 31, 53] and report the discrimination of α versus γ/β events in terms of the discrimination power (DP) at the Q-value for $0\nu\beta\beta$ in ^{100}Mo

$$DP = \frac{\mu_\gamma - \mu_\alpha}{\sqrt{\sigma_\gamma^2 + \sigma_\alpha^2}}. \qquad (1)$$

The parameters in the definition of the DP are the mean RLYs μ_α, μ_γ for α and γ/β events respectively, and resolutions σ_α, σ_γ. We obtain detector based RLYs $\mu_\alpha = QF_\alpha \cdot \mu_\gamma$ from the measured RLYs μ_γ and approximate the very uniform light quenching of α events with $QF_\alpha = 0.2$ (see Table 3). The expected LD resolutions σ_α and σ_γ at the endpoint of the ^{100}Mo decay are extrapolated by adding the baseline resolution and a statistical photon noise component with an average photon energy of 2.07 eV [53] in quadrature. The resulting median discrimination power is 15.0, with the worst-performing detector having a discrimination power of 6.3. Hence all detectors are expected to achieve better than 99.9% α rejection with more than 99.9% γ/β acceptance.

We note that this model calculation does not take into account additional sources of uncertainty such as variation associated with the position of the incident particle interaction and subsequent light propagation. However, the validity of the model is supported by the excellent agreement between the predicted and achieved discrimination in neutron calibration data in previous measurements[31]. The computed discrimination level exceeds the requirements for CUPID, and

we plan to study adverse effects due to non-Gaussian tails with larger statistics in the future. If multiple alpha peaks emerge in individual detectors we will also be able to study the α energy scale and the energy dependence of the α discrimination from data. It should be noted that we are only using a single of the two LDs (see sec. 3.4). As a result, even in the presence of non-Gaussian tails, or additional energy dependent effects, information from the combination of the LDs could be used to improve the discrimination.

Table 3 Performance of ^{100}Mo-enriched Li_2MoO_4 bolometers of the CUPID-Mo experiment operated at 20.7 mK in the EDELWEISS set-up at LSM (France). This table contains the following information: the crystals size and mass, the NTD resistance at the working point (R_{work}), the rise-time (τ_R), the decay-time (τ_D), the voltage sensitivity (A_{Signal}), the baseline noise resolution (FWHM$_{Noise}$), the scintillation light yield (RLY) measured by top LD (RLY_{top}) and bottom LD (RLY_{bottom}), and the light yield quenching for alpha particles (QF_α). The omission of a measured parameter due to lack of statistics or insufficient detector performance is indicated by "–". The median value for RLY_{bottom} is given for scintillators coupled to two LDs (^{a}) and for single LD (^{b}); see text.

enrLMO ID	Size (mm)	Mass (g)	R_{work} (MΩ)	τ_R (ms)	τ_D (ms)	A_{Signal} (nV/keV)	FWHM$_{Noise}$ (keV)	RLY_{top} (keV/MeV)	RLY_{bottom} (keV/MeV)	QF_α (%)
1	⌀43.6 × 40.0	185.86	1.37	31	476	10	2.01	0.67	0.66	19.5
2	⌀43.6 × 44.2	203.72	1.04	48	1093	1.2	30.6	n.a.	0.96	20.8
3	⌀43.9 × 45.6	212.61	0.75	33	302	14	2.56	0.83	–	–
4	⌀43.9 × 44.5	206.68	1.07	29	264	25	2.23	0.61	0.56	21.4
5	⌀43.8 × 45.0	211.10	1.77	19	584	21	1.52	n.a.	0.80	18.6
6	⌀43.8 × 45.0	209.19	1.69	23	384	25	3.62	0.65	0.64	19.1
7	⌀43.8 × 45.0	210.45	0.85	24	357	21	1.15	0.77	–	20.9
8	⌀43.8 × 45.0	209.71	1.53	29	406	24	1.04	–	0.60	–
9	⌀43.8 × 45.3	209.30	0.69	28	464	13	4.48	n.a.	0.90	19.6
10	⌀43.8 × 45.3	208.90	1.94	32	341	28	0.98	0.75	0.66	21.8
11	⌀43.8 × 45.3	208.18	2.99	18	173	23	1.70	0.74	0.61	17.7
12	⌀43.8 × 45.4	209.98	3.76	21	213	15	1.85	0.75	0.65	18.9
13	⌀43.8 × 45.5	210.35	1.37	25	445	15	4.62	n.a.	0.91	19.2
14	⌀43.8 × 44.5	205.76	1.16	15	95	15	3.77	0.63	0.55	20.6
15	⌀43.7 × 45.2	209.50	1.24	28	195	6	4.98	0.65	0.58	18.8
16	⌀43.8 × 45.0	208.96	1.38	21	228	20	1.47	0.67	0.58	21.0
17	⌀43.8 × 45.3	209.20	1.51	24	292	23	1.94	n.a.	0.80	20.1
18	⌀43.8 × 45.3	210.09	2.22	18	192	17	2.09	0.77	0.64	20.0
19	⌀43.8 × 45.3	209.16	1.36	20	173	18	1.38	0.76	0.68	20.4
20	⌀43.8 × 45.3	209.70	2.48	14	97	17	1.89	0.67	0.66	19.2
Median	⌀43.8 × 45.3	208.54	1.37	24	297	17	1.97	0.74	0.64^b 0.90^b	19.8

3.7 Radiopurity of $Li_2{}^{100}MoO_4$ crystals

We apply an additional anticoincidence cut with a time coincidence window of 100 ms between Li_2MoO_4 detectors, a so called multiplicity one (M1) cut to reject multi-Compton and muon shower events and obtain the background spectrum shown in Fig. 16. The γ/β spectrum of $Li_2{}^{100}MoO_4$ bolometers above ~ 1 MeV is dominated by the $2\nu 2\beta$ decay of ^{100}Mo with an activity of 10 mBq/kg[1]. In 11.1 days of background data, we observe no event compatible with the RLY of γ/β events above 3034 keV, the Q-value for double beta decay in ^{100}Mo. The estimate for the resolution at 2615 keV, (6.5 ± 1.4) keV, is compatible with the prediction from the calibration data, albeit this is subject to considerable uncertainty due to the limited statistics.
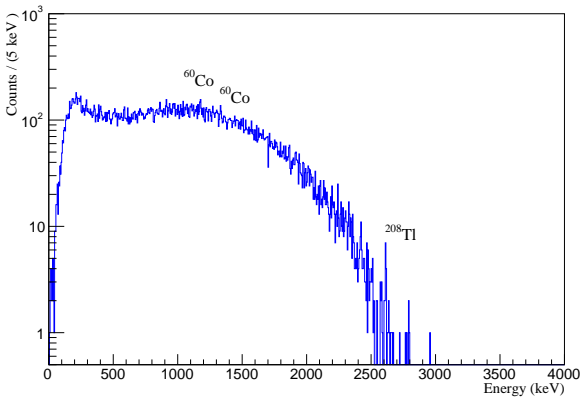
Fig. 16 Summed background spectrum using 11.1 days of data from 19/20 $Li_2{}^{100}MoO_4$ cryogenic detectors of the CUPID-Mo experiment.

By relaxing the pulse shape cuts, and removing the γ/β LY cuts and the M1-cut, we can investigate the α region with a set of basic cuts that are designed to have better than 99% acceptance. The only clear contaminants seen in the spectrum (see Fig. 17) are a bulk and surface peak by ^{210}Po (^{210}Pb), as observed in the LUMINEU studies [1, 31]. For a few of the nuclei in the Th- (^{232}Th, ^{228}Th, ^{224}Ra, ^{212}Bi) and the U-chain (^{238}U, $^{234}U + ^{226}Rn$, ^{230}Th, ^{222}Rn, ^{218}Po), that have a clean decay signature we start to see first hints of a contamination. However, the number of events in a ± 30 keV window around the nominal decay energy is compatible with 0 at the 2 σ level for all of the decay signatures. We thus place a conservative upper limit at a level of 2 μBq/kg (Th-series) and 3 μBq/kg (U-series) (90% C.L.) on the activity in the U-/Th-chains using the largest observed event count for any of the decays in the U-/Th-chain.

We look for possible backgrounds from surface contaminants in the 3–4 MeV region. Excluding a potential ^{190}Pt alpha bulk contribution in a ± 30 keV window around 3269 keV we observe 14 events, which is equivalent to a background of (0.14 ± 0.04) counts/(keV$\times$kg$\times$yr) in degraded alpha events before the rejection by RLY.
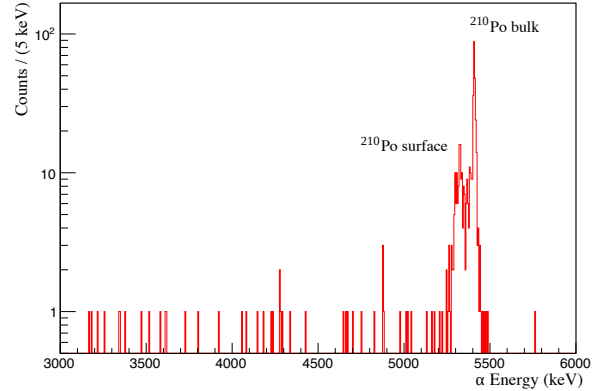

Fig. 17 Summed alpha region using 19/20 detectors. No LY cut applied. (For details see text.)

4 Outlook

Based on these first physics data we are confident that the $Li_2{}^{100}MoO_4$ cryogenic detectors possess a high degree of reproducibility and are well suited to scale to a much larger CUORE sized detector array in CUPID [5]. We expect the current CUPID-Mo experiment to be able to set significant limits on $0\nu\beta\beta$ in ^{100}Mo. We evaluate the CUPID-Mo sensitivity using the Bayesian method for limit setting for a counting experiment in a $\pm 2\sigma$ region of interest around $Q_{\beta\beta}$. At present, several steps of the data analysis procedure have not been fully optimized, leaving room for improvement. We expect to achieve a 5 keV energy resolution with a dedicated optimization of the energy reconstruction algorithms. With an average containment efficiency for $0\nu\beta\beta$ decay events of 75%, and assuming an $\sim 90\%$ analysis efficiency, as obtained in CUORE [6] and CUPID-0 [29] for the combined trigger efficiency, multiplicity, pulse shape analysis (PSA) and LY cut efficiencies we obtain the exclusion sensitivity curves reported in Fig. 18. If we demonstrate a background index of 10^{-2} counts/(keV$\times$kg$\times$yr) with increased statistics, CUPID-Mo reaches a sensitivity superior to the most recent limit on the ^{100}Mo half-life set by NEMO-3 [36] in just 6 months of accumulated livetime. Fig. 18 also reports the sensitivity for the more optimistic scenario where the background level is 10^{-3} counts/(keV$\times$kg$\times$yr); in this case, the experiment is practically background free for a total of 1 yr of livetime reaching a final sensitivity of 2.43×10^{24} yr. The exclusion sensitivity has a very minor dependence on the detector energy resolution and decreases by $\sim 10\%$ for a factor two worse resolution and a background index of 10^{-2} counts/(keV$\times$kg$\times$yr).
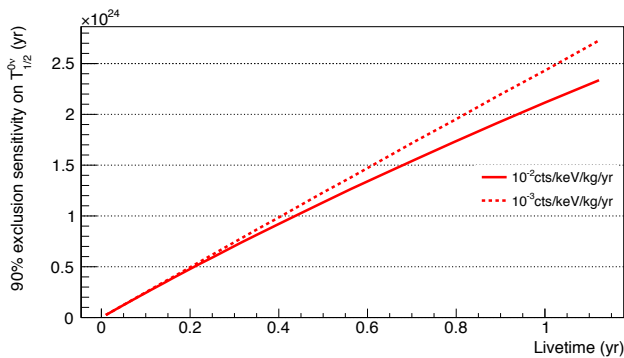
Fig. 18 Bayesian exclusion sensitivity at 90% C.I. for 5 keV resolution, and different background levels.

5 Conclusion

The first physics data of the CUPID-Mo experiment validates and extends the previously reported bolometric performance for cryogenic Li_2MoO_4 crystals [1, 31] on a much larger array of 20 detectors. We find that crystal growth and detector assembly can be well controlled to obtain excellent uniformity in performance and radiopurity. In particular, the summed energy resolution was 5.3 keV (6.5 keV) FWHM at 2615 keV in calibration (physics) data of 19 out of 20 detectors. The measured light yield for γ/β events (0.6–0.9 keV/MeV), the quenching of the scintillation light for alpha particles (20%) with respect to γ/βs and the achieved baseline resolution of bolometric Ge light detectors (146 eV FWHM) are compatible with full α to γ/β separation (15σ median value). The results indicate the prospect to surpass the sensitivity of NEMO-3 with $\sim$6 months of physics data in the current demonstrator. The technology is scalable, and the first results presented in this article strengthen the choice of $Li_2{}^{100}MoO_4$ as the baseline option for application in the CUPID next-generation cryogenic $0\nu\beta\beta$ experiment. Additional data from the current and future demonstrators is essential to develop a detailed background model, investigate and optimize the performance in the region of interest for $0\nu\beta\beta$, and to strengthen the projections for CUPID further.

References

1. E. Armengaud, et al., Eur. Phys. J. C **77**, 785 (2017)
2. G. Wang, et al., arXiv:1504.03612 (2015)
3. G. Wang, et al., arXiv:1504.03599 (2015)
4. D.R. Artusa, et al., Eur. Phys. J. C **74**, 3096 (2014)
5. W.R. Armstrong, et al., arXiv:1907.09376 (2019)
6. C. Alduino, et al., Phys. Rev. Lett. **120**, 132501 (2018)
7. M. Goeppert-Mayer, Phys. Rev. **48**, 512 (1935)
8. A.S. Barabash, Nucl. Phys. A **935**, 52 (2015)
9. A.S. Barabash, arXiv:1907.06887 (2019)
10. J.D. Vergados, H. Ejiri, F. Simkovic, Int. J. Mod. Phys. E **25**, 1630007 (2016)
11. S. Dell'Oro, S. Marcocci, M. Viel, F. Vissani, Adv. High Energy Phys. **2016**, 2162659 (2016)
12. S.M. Bilenky, C. Giunti, Int. J. Mod. Phys. A **30**, 1530001 (2015)
13. F.F. Deppisch, M. Hirsch, H. Pas, J. Phys. G **39**, 124007 (2012)
14. W. Rodejohann, J. Phys. G **39**, 124008 (2012)
15. M. Fukugita, T. Yanagida, Phys. Lett. B **174**, 45 (1986)
16. J. Schechter, J.W.F. Valle, Phys. Rev. D **25**, 2951 (1982)
17. A. Gando, et al., Phys. Rev. Lett. **117**, 082503 (2016)
18. J.B. Albert, et al., Phys. Rev. Lett. **120**, 072701 (2018)
19. C.E. Aalseth, et al., Phys. Rev. Lett. **120**, 132502 (2018)
20. M. Agostini, et al., Phys. Rev. Lett. **120**, 132503 (2018)
21. E. Fiorini, T. Niinikoski, Nucl. Instrum. Meth. A **224**, 83 (1984)
22. D. Poda, A. Giuliani, Int. J. Mod. Phys. A **32**, 1743012 (2017)
23. C. Alduino, et al., Eur. Phys. J. C **77**, 532 (2017)
24. C. Alduino, et al., Eur. Phys. J. C **77**, 543 (2017)
25. S. Pirro, et al., Phys. Atom. Nucl. **69**, 2109 (2006)
26. S. Rahaman, et al., Phys. Lett. B **662**, 111 (2008)
27. D.L. Lincoln, et al., Phys. Rev. Lett. **110**, 012501 (2013)
28. O. Azzolini, et al., Eur. Phys. J. C **78**, 428 (2018)
29. O. Azzolini, et al., Phys. Rev. Lett. **123**, 032501 (2019)
30. O. Azzolini, et al., Eur. Phys. J. C **79**, 583 (2019)
31. D.V. Poda, et al., AIP Conf. Proc. **1894**, 020017 (2017)

32. E. Armengaud, et al., JINST **12**, P08010 (2017)
33. L. Hehn, et al., The European Physical Journal C **76**(10), 548 (2016)
34. L. Bergé, et al., JINST **9**, P06004 (2014)
35. V.D. Grigorieva, et al., J. Mat. Sci. Eng. B **7**, 63 (2017)
36. R. Arnold, et al., Phys. Rev. D **92**, 072011 (2015)
37. M. Mancuso, et al., EPJ Web Conf. **65**, 04003 (2014)
38. E.E. Haller, Infrared Phys. Techn. **35**, 127 (1994)
39. E. Andreotti, et al., Nucl. Instrum. Meth. A **664**, 161 (2012)
40. A. Alessandrello, et al., J. Cryst. Growth **412**, 454 (1998)
41. B. Schmidt, et al., Astropart. Phys. **44**, 28 (2013)
42. Q. Arnaud, et al., Phys. Rev. D **97**, 022003 (2018)
43. D.L. Helis, et al., Submitted to J. Low Temp. Phys. (2019)
44. D.V. Poda, ^{100}Mo-enriched Li_2MoO_4 scintillating bolometers for $0\nu2\beta$ decay search: from LUMINEU to CUPID-0/Mo projects. URL http://medex17.utef.cvut.cz/talks/Poda.pdf. Talk given at 11th Int. Conf. MEDEX'2017, Prague, Czech Republic, May 29 – June 02, 2017
45. L. Bergé, et al., Phys. Rev. C **97**, 032501(R) (2018)
46. E. Gatti, P. Manfredi, Riv. Nuovo Cim. **9**, 1 (1986)
47. C. Alduino, et al., Phys. Rev. C **93**, 045503 (2016)
48. O. Azzolini, et al., Eur. Phys. J. C **78**, 734 (2018)
49. M. Mancuso, Development and optimization of scintillating bolometers and innovative light detectors for the search for neutrinoless double beta decay. Ph.D. thesis, University Paris-Sud, Orsay, France (2016). URL https://hal.inria.fr/tel-01315155
50. M. Stonebraker, L.A. Rowe, SIGMOD Rec. **15**(2) (1986)
51. A.C. Thompson, et al., *X-ray Data Booklet* (Lawrence Berkeley National Laboratory, University of California Berkeley, 2009). URL http://xdb.lbl.gov/xdb-new.pdf
52. M. Barucci, et al., Nucl. Instrum. Meth. A **935**, 150 (2019)
53. T.B. Bekker, et al., Astropart. Phys. **72**, 38 (2016)